Developmental Cognitive Neuroscience 63 (2023) 101284

Contents lists available at ScienceDirect

Developmental Cognitive Neuroscience

journal homepage: www.elsevier.com/locate/dcn

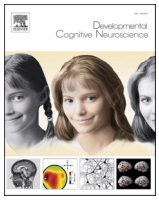

Mapping the evolution of regional brain network efficiency and its association with cognitive abilities during the first twenty-eight months of life

Weixiong Jiang [a], Zhen Zhou [a], Guoshi Li [a], Weiyan Yin [a], Zhengwang Wu [a], Li Wang [a], Maryam Ghanbari [a], Gang Li [a], Pew-Thian Yap [a], Brittany R. Howell [b], Martin A. Styner [c], Essa Yacoub [d], Heather Hazlett [c,e], John H. Gilmore [c], J. Keith Smith [e], Kamil Ugurbil [d], Jed T. Elison [b,f], Han Zhang [g], Dinggang Shen [g,h], Weili Lin [a,*]

[a] Department of Radiology and BRIC, University of North Carolina at Chapel Hill, Chapel Hill, NC 27599, USA
[b] Institute of Child Development, University of Minnesota, USA
[c] Department of Psychiatry, University of North Carolina at Chapel Hill, USA
[d] Center for Magnetic Resonance Research, University of Minnesota, USA
[e] Department of Radiology, University of North Carolina at Chapel Hill, USA
[f] Department of Pediatrics, University of Minnesota, USA
[g] Biomedical Engineering, Shanghai Tech University, Shanghai, China
[h] Shanghai Clinical Research and Trial Center, Shanghai 201210, China

ARTICLE INFO

Keywords:
Longitudinal
Development
Brain network
Graph theory
RsfMRI
Cognitive ability

ABSTRACT

Human brain undergoes rapid growth during the first few years of life. While previous research has employed graph theory to study early brain development, it has mostly focused on the topological attributes of the whole brain. However, examining regional graph-theory features may provide unique insights into the development of cognitive abilities. Utilizing a large and longitudinal rsfMRI dataset from the UNC/UMN Baby Connectome Project, we investigated the developmental trajectories of regional efficiency and evaluated the relationships between these changes and cognitive abilities using Mullen Scales of Early Learning during the first twenty-eight months of life. Our results revealed a complex and spatiotemporally heterogeneous development pattern of regional global and local efficiency during this age period. Furthermore, we found that the trajectories of the regional global efficiency at the left temporal occipital fusiform and bilateral occipital fusiform gyri were positively associated with cognitive abilities, including visual reception, expressive language, receptive language, and early learning composite scores ($P < 0.05$, FDR corrected). However, these associations were weakened with age. These findings offered new insights into the regional developmental features of brain topologies and their associations with cognition and provided evidence of ongoing optimization of brain networks at both whole-brain and regional levels.

1. Introduction

The first few years of life mark a period of exceptional structural and functional development in the human brain, exerting profound and long-lasting impacts on cognitive abilities later in life (Gilmore et al., 2018). Magnetic resonance imaging (MRI) has been widely used to gain insights into both the structural and functional development of the brain during this critical period. Anatomical MR images have revealed substantial increases in brain volume (Gao et al., 2017; Peterson et al., 2021), expansion of regional surface area (Huang et al., 2022; Cafiero et al., 2019), and developmental trajectories of cortical thickness (Wang et al., 2019; Nie et al., 2014). Diffusion tensor imaging (DTI), a technique that provides insights into white matter microstructures, has revealed the rapid process of myelination and the establishment of white matter connectome (Bagonis et al., 2022; Cafiero et al., 2019; Tymofiyeva et al., 2013; Yap et al., 2011). Resting-state functional MRI

* Correspondence to: Department of Radiology and BRIC CB#7513, University of North Carolina at Chapel Hill, Chapel Hill, NC 27599-7513, USA.
E-mail address: Weili_lin@med.unc.edu (W. Lin).

https://doi.org/10.1016/j.dcn.2023.101284

Available online 27 July 2023

(rsfMRI) has been utilized to establish brain functional networks, uncovering temporal progression of various cognitive domains (Gao et al., 2017; Gilmore et al., 2018; Zhang et al., 2019). Together, these complementary techniques have provided valuable insight into early brain development.

While numerous studies have reported the developmental features of brain functional networks from early infancy to young childhood (Bruchhage et al., 2020; Emerson et al., 2016; Eyre et al., 2021; Gao et al., 2015; Gao et al., 2009; Wen et al., 2020), graph-theory analyses of brain networks offer additional insights into the evolution of brain network topologies (Gao et al., 2011; Wen et al., 2019; Yin et al., 2019; Zhao et al., 2019a). A "small-world" topology, characterized by an efficient and interconnected network architecture with high clustering coefficients and short path lengths (Humphries and Gurney, 2008), has been found to already exist at birth (De Asis-Cruz et al., 2015; Fransson et al., 2011). Whole-brain global efficiency (GE), a measure of the brain's ability to transfer information across the whole brain (Wang et al., 2009), continues to increase during the first year (Berchicci et al., 2015; Gao et al., 2011) and remains relatively stable during the second year of life (Gao et al., 2011). In contrast, the reported results on local efficiency (LE), which characterizes the efficiency of information transfer within local neighborhoods (Wang et al., 2009), have been less consistent (Fan et al., 2011; Gao et al., 2011; Huang et al., 2015; Nie et al., 2014; Yap et al., 2011) and even contradictory in some cases using structural MRI (Fan et al., 2011; Nie et al., 2014). The better developmental consistency observed in GE when compared to LE can be attributed to GE's ability to capture the overall integration of information in the brain network, making it less sensitive to local or individual variance. In contrast, LE could be more susceptible to local variations and specific characteristics of individual nodes or other factors, such as differences of study cohort characteristics, varying imaging protocols and analytical approaches, as well as the dynamic nature of individual brain development. Furthermore, it is worth mentioning that previous studies have mainly utilized a cross-sectional design (De Asis-Cruz et al., 2015; Gao et al., 2011; Huang et al., 2015; Ratnarajah et al., 2013), which may have limitations due to variations in brain connectivity and developmental trajectories among individuals. Although a few longitudinal studies have been employed to better capture developmental features at the individual level, the sample sizes have been relatively small (Huang et al., 2015; Nie et al., 2014; Yap et al., 2011). In addition, previous studies have mainly reported results at the *whole brain or network* levels using graph theory (De Asis-Cruz et al., 2015; Ratnarajah et al., 2013; Yap et al., 2011; Zhao et al., 2019a). It is well understood that distinct cognitive functions are governed by specific regions of the brain. Thus, regional graph theory attributes may be more sensitive to capturing specific behavioral and cognitive abilities when compared to global attributes.

In this study, we conducted a comprehensive analysis by leveraging a large longitudinal rsfMRI data from the UNC/UMN Baby Connectome Project (BCP) (Howell et al., 2019) to investigate fine-grained whole-brain and regional efficiency developmental trajectories, and to test two hypotheses: 1) developmental patterns of regional network attributes are spatially heterogeneous and reflect unique functional roles of different brain regions, and 2) developmental attributes of specific brain regions are associated with early cognitive ability. To achieve these goals, we investigated the characteristics of regional efficiency and reported the developmental trajectories of regional global efficiency (rGE) and local efficiency (rLE) from infancy to toddlerhood. Our findings suggested that the developmental trajectories of regional efficiency attributes may reflect specific functional roles. Specifically, we observed that brain regions involved in sensorimotor functions, primary visual regions, and high-order visual and subcortical regions exhibited linear, logarithmic (log), and quadratic development trajectories, respectively. Moreover, we found that the rGE developmental attributes at the fusiform cortex were associated with cognitive abilities, highlighting the potential relations between regional network attributes and cognition.

2. Materials and methods

2.1. Data acquisition

All subjects included in this study were enrolled in the UNC/UMN Baby Connectome Project, and all images were collected using 3 T Siemens Prisma MRI scanners. The inclusion criteria were as follows: 1) young children born at a gestational age of 37 – 42 weeks, 2) with a birth weight appropriate for gestational age, 3) without major pregnancy and delivery complications. Major delivery complications may include neonatal hypoxia or neonatal illness requiring a NICU stay of more than two days. 4) not adopted, 5) without a first degree relative with autism, intellectual disability, schizophrenia, or bipolar disorder, 6) without any significant medical and/or genetic conditions affecting growth, development, or cognition, 7) without any contraindication to MRI, or major pre- and/or perinatal issues such as maternal pre-eclampsia, placental abruption, maternal HIV status, or maternal alcohol or illicit drug use during pregnancy, and 8) their caregivers are able to communicate in English at a level to provide informed consent (Howell et al., 2019).

All subjects were imaged without sedation and during natural sleep. A single-shot echo-planar imaging (EPI) sequence was used to acquire rsfMRI with the following parameters: repetition time (TR) = 800 ms, echo time (TE) = 37 ms, flip angle (FA) = 52°, slice number/orientation = 72/axial oblique, field of view (FOV) = 208 × 208 mm^2, multi-band factor = 8, matrix size = 104 × 104, and resolution= 2 × 2 × 2 mm^3. T1-weighted (MPRAGE) images were acquired to provide structural information with the following parameters: TR/TI = 2400/1060 ms, TE = 2.24 ms, FA = 8°, slice number/orientation = 208/sagittal, FOV = 256 × 240 mm^2, matrix size = 320 × 300, and resolution= 0.8 × 0.8 × 0.8 mm^3. The FIRMM (framewise integrated real-time MRI monitoring) software was used to monitor subject's motion during rsfMRI acquisition (Dosenbach et al., 2017); images with visible movement were excluded and rsfMRI scans were repeated. For each visit, two to four rsfMRI runs were conducted, which included both anterior-to-posterior (AP) and posterior-to-anterior (PA) phase encoding and repeated AP/PA runs.

The Mullen Scales of Early Learning (MSEL) was used to assess cognitive ability of each subject within a month of their MRI visit. The MSEL is a comprehensive assessment of cognitive ability for infants and young children up to 68 months of age (Mullen, 1995; Yitzhak et al., 2016). The assessment comprises five subdomain cognitive scales: visual reception (VR), fine motor (FM), expressive language (EL), receptive language (RL), and gross motor (Mullen, 1995). The early learning composite (ELC) score is a composite of the first four subdomain scores (Mullen, 1995). The age-normalized *T* scores from each subscale of the MSEL were used in this study (Mullen, 1995). For subjects who underwent multiple MSEL assessments at different ages, the *T*-score of each cognitive score at the last visit was employed for subsequent analyses (Mullen, 1995).

2.2. Data preprocessing

The rsfMRI data were pre-processed using a specific pipeline designed for young children (Jiang et al., 2019; Wang et al., 2015; Wang et al., 2023; Wu et al., 2012). This pipeline shares several similar steps as those of the Human Connectome Project (HCP) pipeline (https://github.com/Washington-University/Pipelines), but it also includes several unique steps tailored to young children's rsfMRI data. Specifically, the following strategies were employed. First, one-time resampling and denoising were conducted in each subject's native space and the topological attribute maps were calculated in the individual native space and aligned with the corresponding anatomical images. The Montreal Neurological Institute (MNI) template was warped to each subject's native space to minimize difficulties in selecting the smoothing kernel and reduce partial volume effects when infant and toddler data were registered to the standard MNI space. Second, brain tissue segmentation was performed using iBEAT V2.0 (http://www.ibeat.cloud) to generate

brain tissue labeling maps. Each voxel was labeled as gray matter, white matter, or cerebrospinal fluid (Wang et al., 2023). The tissue labeling maps were then used to register to the tissue labeling template in the MNI space (ICBM_152_t1_tal_nlin_sym09c). This registration method has proven successful in infant and toddler brain volumetric registration by addressing the challenges associated with age-dependent signal intensity and low tissue contrast in anatomical images (Wang et al., 2015; Wu et al., 2012). Lastly, automatic deep learning-based noise-related component removal was adopted for fast and robust rsfMRI denoising (Kam et al., 2019). More detailed descriptions of the employed pre-processing steps were provided in the Supplement Materials.

2.3. Brain network construction

A total of 112 brain regions, both cortical and subcortical, from the Harvard-Oxford atlas were chosen as nodes to construct brain functional networks (Desikan et al., 2006). The BOLD signal of each region was obtained by averaging the signals of all voxels in a given region. The resulting time series of regional averages were used to create a 112 × 112 pairwise FC matrix based on Pearson's correlation (Jiang et al., 2022; Tang et al., 2013; Zhou et al., 2020). These metrics were standardized using Fisher's z-scores and binarized at varying levels of sparsity for positive functional connections. Specifically, an FC threshold was chosen for each sparsity such that if the FC between two regions exceeded the threshold, it was set to 1; otherwise, it was set to 0, indicating the absence of a functional connection between them. The corresponding abbreviations of the 112 brain regions can be found in Table S1.

Small-world networks are characterized by high clustering coefficients (functional segregation) and short characteristic path lengths (functional integration) (Bassett and Bullmore, 2017; Watts and Strogatz, 1998). To ensure that all analyses were conducted under small-world conditions, the small-world metric was calculated for all subjects at various network sparsity levels ranging from 1% to 80% with a step of 1%. More information on the calculation of the small-world index is provided in the Supplement Materials.

2.4. Regional network efficiency

In this study, we analyzed GE and LE at both the whole-brain and regional levels. The whole-brain GE reflects the overall flow of information across the entire network, while LE assesses the degree of network segregation (Wang et al., 2009). At the regional level, the regional GE (rGE) evaluates a region's ability to transfer information with all other regions in the network, while the regional LE (rLE) measures the efficiency of information exchange among a region's immediate neighbors without considering its own connectivity (Latora and Marchiori, 2001; Wang et al., 2009). Here, "neighbors" refers to the nodes that are directly connected to the examined node. The whole brain GE and LE values were calculated as the average of the rGE (rLE) values of all regions in the brain, respectively. Specifically, the rGE of a given node (region) i is defined as:

$$E(i) = \frac{1}{n-1}\sum_{j\in G, j\neq i}\frac{1}{d(i,j)}, \tag{1}$$

where n denotes the number of total nodes in a network G and $d(i,j)$ denotes the shortest path length between nodes i and j.

The rLE of a given node i is defined as the GE of a local subgraph,

$$E_{loc}(i) = E(G_i), \tag{2}$$

where G_i consists only of the node's immediate neighbors but not the node itself.

To avoid biases when a specific sparsity threshold was used for network binarization, the area under each metric's curve (AUC) over the sparsity range exhibiting small-world topologies was used for the subsequent analyses (Eq. (3)). The calculated network attributes were averaged from different resting-state runs during the same visit of the same subject (Cao et al., 2019).

$$AUC\_E = \left(\sum_{i=1}^{N} E_i - (E_1 + E_N)/2\right) * AUC\_Interval \tag{3}$$

where E_i represents each global/regional attribute of a binary network at each sparsity value $i = [1, 2, \ldots, N]$ and *AUC_Interval* is the step of 1%.

2.5. Characterization of longitudinal developmental trajectories

The developmental trajectories of global and regional metrics were analyzed quantitatively using the linear mixed effect regression (LMER) models, with the chronological age in days as the variable. Three age models were used to characterize different developmental trajectories, including linear, logarithmic, and quadratic age models, as defined below. We avoided using polynomials with high degrees to prevent overfitting (Ziegler et al., 2012).

$$y_{ij} = \beta_0 + \beta_1(\mathrm{Age}_{ij}) + (b_{0i} + b_{1i}(\mathrm{Age}_{ij}) + \varepsilon_{ij}), \tag{4}$$

$$y_{ij} = \beta_0 + \beta_1(\ln(\mathrm{Age}_{ij})) + (b_{0i} + b_{1i}(\ln(\mathrm{Age}_{ij})) + \varepsilon_{ij}) \tag{5}$$

and

$$y_{ij} = \beta_0 + \beta_1(\mathrm{Age}_{ij}) + \beta_2\left(\mathrm{Age}_{ij}^2\right) + (b_{0i} + b_{1i}(\mathrm{Age}_{ij}) + \varepsilon_{ij}), \tag{6}$$

where the dependent variable y_{ij} denotes each global/regional efficiency attribute for subject $i = [1, 2, \ldots, N]$ at the time point $j = [1, 2, \ldots, n_i]$, and the independent variable *Age* denotes the corresponding age (in days). β_0 and β_k ($k = 1, 2$) respectively denote the group-level intercept and the k^{th} regression coefficient, while b_{0i} and b_{1i} denote the random intercepts and slopes, respectively, that characterize the individual effects (individually specific developmental pattern that deviates from the group-level pattern). Finally, ε_{ij} denotes the random errors of the model and *ln* denotes logarithm.

The Akaike information criterion (AIC) was used to select the best fitted model among the three models (King, 2016). Significance was set at $P < 0.05$ after correction for multiple comparisons using false discovery rate (FDR). The P value of β_k ($k = 1, 2$) was used to evaluate the significance of developmental trajectories when compared to a horizontal line.

2.6. Variations in regional efficiency across age groups

To further investigate the potential variations in regional efficiency across different ages, we separated our data into age groups with an interval of three months to prevent repeated visits from the same subjects within a group. We employed paired t-tests to compare each region's rGE/rLE with individual whole-brain average to identify brain regions that were significantly different from the whole brain GE/LE at the group level in each age group. Lastly, we used two-sample t-tests to compare rGE/rLE between adjacent age groups. Their significance levels were consistently set as $P < 0.05$ after FDR correction.

2.7. Associations between cognition and network efficiency

To investigate potential associations between cognition and network efficiency, LMER models were employed, with each Mullen subdomain score and the ELC as variables, respectively, while controlling for sex and site (UNC or UMN). Both linear and log cognitive models were applied to assess global and local efficiency at both whole-brain and regional levels. Specifically, for regional analyses, we focused on brain regions that demonstrated significant age effects based on the aforementioned linear and nonlinear age models.

$$y_{ij} = \beta_0 + \beta_1(Sex_i) + \beta_2(S_i) + \beta_3(CogScore_i) + \beta_4\left(\mathrm{Age}_{ij}\right) + \beta_5\left(\mathrm{Age}_{ij} \bullet CogScore_i\right) + \left(b_{0i} + b_{1i}\left(\mathrm{Age}_{ij}\right) + \varepsilon_{ij}\right), \quad (7)$$

$$y_{ij} = \beta_0 + \beta_1(Sex_i) + \beta_2(S_i) + \beta_3(CogScore_i) + \beta_4\left(\ln(\mathrm{Age}_{ij})\right) + \beta_5\left(\ln(\mathrm{Age}_{ij}) \bullet CogScore_i\right) + \left(b_{0i} + b_{1i}\left(\ln(\mathrm{Age}_{ij})\right) + \varepsilon_{ij}\right), \quad (8)$$

where S denotes sites. CogScore represents cognitive scores, including the EL, FM, RL, VR, GM, and ELC. Here, we not only investigated the unique influence of each MSEL sub-score on whole-brain and regional attributes, but also explored the interactions between age and each MSEL score (Hedeker and Gibbons, 2006). In each model, we regressed the influence of sex, site, and age. We set the significance level as $P < 0.05$ after FDR correction for both the number of brain regions and the number of cognitive measures. The P values of β_3 and β_5 were used to evaluate the significance of cognitive influence on the intercept and the interaction between each MSEL score and age or the significance of cognitive influence on developmental rate, respectively. A quadratic model was not considered as the interactive effect could be complicated (including quadratic term x^2 and first-time term x) and difficult to interpret biologically.

3. Results

3.1. Study cohort

In total, 269 subjects and 1562 rsfMRI runs were included in this study. Seven runs with inadequate brain coverage or inconsistent imaging parameters, and 116 runs from 71 subjects with excessive head motion (FD $\geq$ 0.5 mm) (Power et al., 2012) were excluded. Furthermore, since there were only a few observations after 28 months old (Fig. S1), our analyses focused on rsfMRI runs from children younger than 28 months old. The final analysis comprised 1401 rsfMRI runs from 249 subjects with 531 unique visits, as some subjects participated in multiple imaging sessions or were scanned using different phase encoding orientations during the same visit. Fig. 1 illustrates the number of unique visits per subject. Among these rsfMRI runs, the time of scans were available in 1154 scans where 230 (19.93%) were imaged during children's typical daytime naptime, while 924 (80.07%) around their typical bedtime in the night. Finally, of the 249 subjects included in the rsfMRI analysis, 208 had complete Mullen scores. Thus, the association analyses of cognition and network efficiency included 208 subjects with 473 visits. Finally, out of the 166 runs that were excluded from data analyses due to excessive head motion, only two subjects had their rsfMRI runs completely excluded. We assessed the MSEL scores of these two subjects and found that both of them fell within the normal range.

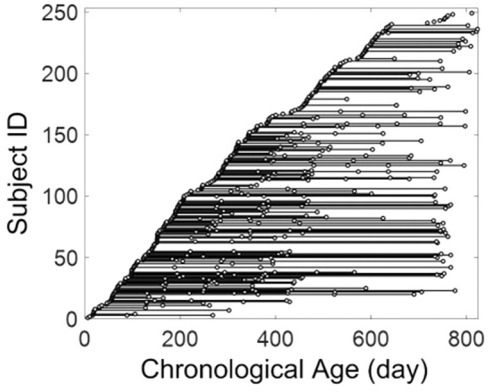

Fig. 1. Distribution of chronological ages for the 249 pediatric subjects included in the study, whose images passed quality control. Each circle represents a successful visit and each line depicts all longitudinal data for an individual subject.

3.2. Developmental trajectory of whole-brain-based network efficiency

The network topology demonstrated small-world characteristics with the sparsity ranging between 17% and 39% for all subjects, as evidenced by a small-world index greater than 1 (Fig. S2) (Wang et al., 2014; Yan and He, 2011). Therefore, the binary FC matrices within the sparsity range of 17–39% with a step of 1% were used for the subsequent analyses.

The efficiency of the whole-brain network demonstrated significant development with age ($P < 0.05$, FDR corrected, Fig. 2 and Table 1). Whole-brain global efficiency increased throughout the age range studied (840 days of age) with a rapid increase during the first few months of life, followed by a gradual and prolonged increase. Local efficiency, on the other hand, followed a quadratic, inverted U-shaped pattern. No significant association was found between the whole-brain network efficiency (GE/LE) and cognitive abilities ($P > 0.05$, FDR corrected).

3.3. Developmental trajectory of region-based efficiency

Regional development trajectories of rGE (Fig. 3A, Table 2) and rLE (Fig. 3B, Table 2) exhibited remarkable spatiotemporal heterogeneity, consistent with our hypothesis. The primary sensorimotor, auditory regions, and bilateral frontal lobe followed a monotonic linear/ log increase of rGE (the first and second column of Fig. 3A) but a log decrease of rLE (the second column of Fig. 3B). The primary (supracalcarine (ScC) and intracalcarine cortex (IcC)) and adjacent higher-order (bilateral lingual gyrus and occipital fusiform gyrus) visual areas showed significantly increased log rGE developmental trajectories (the second column of Fig. 3A), while the temporal/occipital visual areas showed inverted U-shaped quadratic age effects ($P < 0.05$, FDR corrected) (the third column of Fig. 3A). In contrast, these same regions did not show significant rLE development. The quadratic trajectories were also observed in the limbic subcortical cortex for both rGE and rLE (the third column of Fig. 3A and B). Interestingly, the posterior parietal extending to the superior temporal associate areas showed a decreasing log rGE developmental pattern (the second column of Fig. 3A). The developmental trajectories of the brain regions governing basic brain functions were shown in Fig. S3 (Supplement Materials).

The brain regions with different developmental characteristics were merged (fourth column, Fig. 3) and the percentages of brain regions in each model were shown in Fig. 4. Nearly half of the brain regions (48%) showed significant age effects for rGE and 29% for rLE. More brain regions (21%) showed monotonically increasing than monotonically decreasing rGE (8%) with age, while 19% of the brain regions showed a quadratic pattern of rGE. In contrast, 16% of brain regions showed decreasing rLE when compared to 1% of the regions with increasing rLE. Additionally, 12% of the brain regions showed a quadratic pattern of rLE.

To compare the developmental rates of rGE and rLE among different brain regions, we ranked the group-level developmental rate (β_1 *in Eqs.*4*and*5) of different regions calculated by the linear (Fig. 5A (rGE) and 5 C (rLE)) and log models (Fig. S4). The error bars in Fig. 5B and D indicate individual deviation (b_{1i}*in Eqs.*4*and*5). Consistent with the findings shown in Fig. 3, most of the brain regions exhibited a positive developmental rate for rGE but a negative rate for rLE. Additionally, the primary functional areas (sensorimotor and associated visual areas) and prefrontal areas exhibited a faster positive rate of rGE when compared to other brain regions (Table S2), while these areas (except the primary visual areas) showed a faster negative rate of rLE (Table S3).

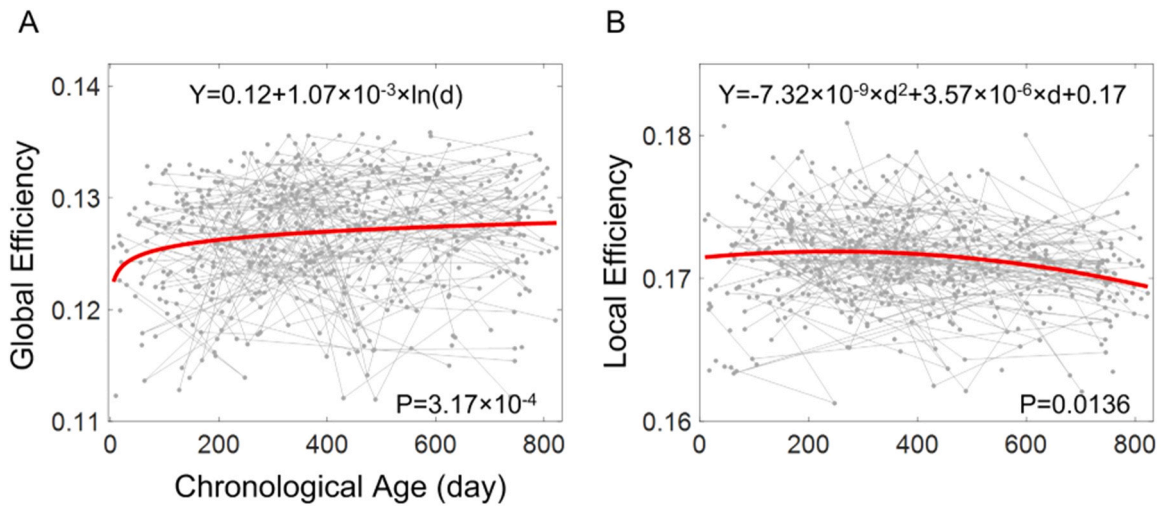

Fig. 2. Developmental trajectories of the whole-brain global (A) and local (B) efficiency in the first 28 months of life. The developmental trajectories of the whole-brain global efficiency (A) were modeled using a log function, while the local efficiency (B) was modeled using a quadratic function.

Table 1
Model Fitting information of whole-brain network efficiency using three models.

	Global Efficiency			Local Efficiency		
	Linear	log	Quadratic	Linear	log	Quadratic
T Values	2.58	3.62	-2.42	-3.96	-2.91	-2.47
P Values	0.0102	3.17E-04	0.0158	8.56E-05	0.0038	0.0136
LCI	6.75E-07	4.90E-04	-2.02E-08	-4.17E-06	-0.0011	-1.31E-08
UCI	4.99E-06	1.65E-03	-2.10E-09	-1.40E-06	-0.0002	-1.51E-09
AIC	-4088	-4095 *	-861	-4587	-4582	-4590 *

*indicates the smallest AIC among the three models. LCI denotes the lower CI bound and UCI denotes the upper CI bound. CI: confidence interval.

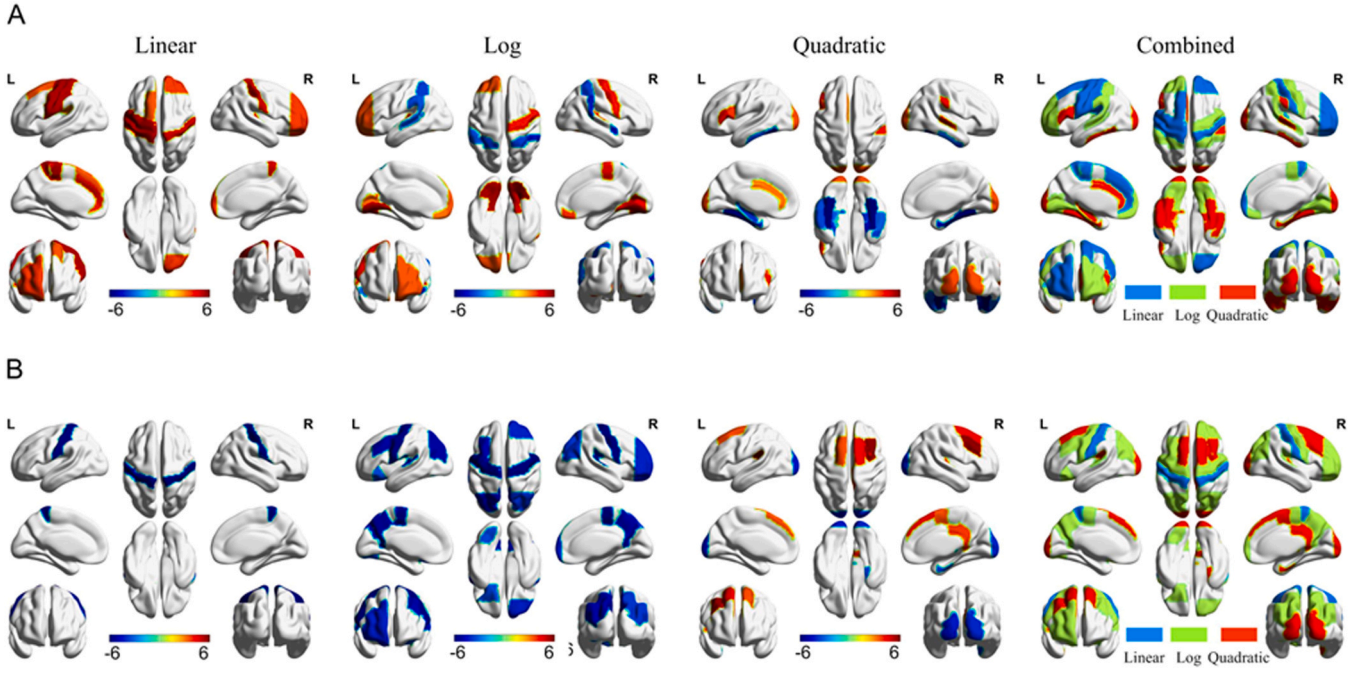

Fig. 3. Significant development of regional global efficiency (A) and regional local efficiency (B). T-values (color bars in columns 1 – 3) of the model fitting are provided after FDR correction ($P < 0.05$). The first, second, and third columns represent results fitted using linear, log, and quadratic models, respectively. Positive and negative T-values indicate increasing and decreasing developmental rates with age for the first and second columns. With the quadratic model (the third column), positive and negative T-values reflect U-shaped and inverted U-shaped development with age. The fourth column illustrates the merged developmental characteristics, showcasing different developmental patterns for each brain region based on the best fitted model. L: left hemisphere; R: right hemisphere.

Table 2
Longitudinal development of regional global and local efficiency after model selection and FDR correction ($P < 0.05$).* .

	Regional Global Efficiency	Regional Local Efficiency
Linear Increase		
L	PoG, PrG, POC, COC, SFG, PcG	ACCU
R	PoG, HesG, FP	
Linear Decrease		
L		PoG, PP
R		PoG, COC
Logarithmic Increase		
L	FMC, IcC, LG, OFG, PUT, ACCU, FP, ScC, HesG	
R	FMC, IcC, LG, OFG, PrG, PP, PT	
Logarithmic Decrease		
L	SPL, SmGp, SmGa, STGp	PrG, PcC, LOCs, PT, COC, HesG, MFG, OFG, FOrC
R	SPL, SmGp	PrG, PcC, LOCs, PT, FP, POC
Quadratic with Inverted U-shape		
L	TOF, TFCp, PhGa, ITGp, PhGp, HIP, ITGt	OcP, PUT
R	TOF, TFCp, PhGa, ITGp, PhGp, ITGa, PUT	OcP, PUT, PhGa, Bstem
Quadratic with U-shape		
L	OcP, CGa, IFGpo, IFGpt	SFG, POC
R	OcP, STGp, SmGa	SFG, JpL, CGp, HesG, MFG

* The abbreviation of each region was provided in Table S1.

3.4. Regional efficiency across age groups

Fig. 6 and Fig. 7 illustrate the brain regions that exhibited significantly different rGE and rLE from the individual whole-brain averages, respectively ($P < 0.05$, FDR corrected). The bilateral precuneus, intraparietal sulcus, temporoparietal junction, and prefrontal regions, displayed a stable and higher rGE than that of the whole brain for all ages. In contrast, the rGE in the limbic regions was consistently lower than that of the whole brain for all ages. Interestingly, the visual cortex displayed a unique pattern: the occipital lobe showed a stable and significantly higher rLE than the whole brain starting from the third month of age. A similar temporal pattern of rLE was also observed in the primary motor and somatosensory regions.

The two-sample t-test between the two adjacent age groups revealed a significant increase of rGE in the precuneus and fusiform ($P < 0.05$, FDR corrected) during the first six months of life (Fig. 6, first row). Meanwhile, a significant increase of rLE in the occipital regions and a decrease of rLE ($P < 0.05$, FDR corrected) were observed in the frontal lobe during the same period (Fig. 7, first row).

3.5. Associations between cognitive ability and regional efficiency

Both the linear and log cognitive models revealed the same brain regions where the development of regional global efficiency was associated with cognitive scores. The results are summarized in Table 3 using the log model (Table S4 for the linear model). The left temporal occipital

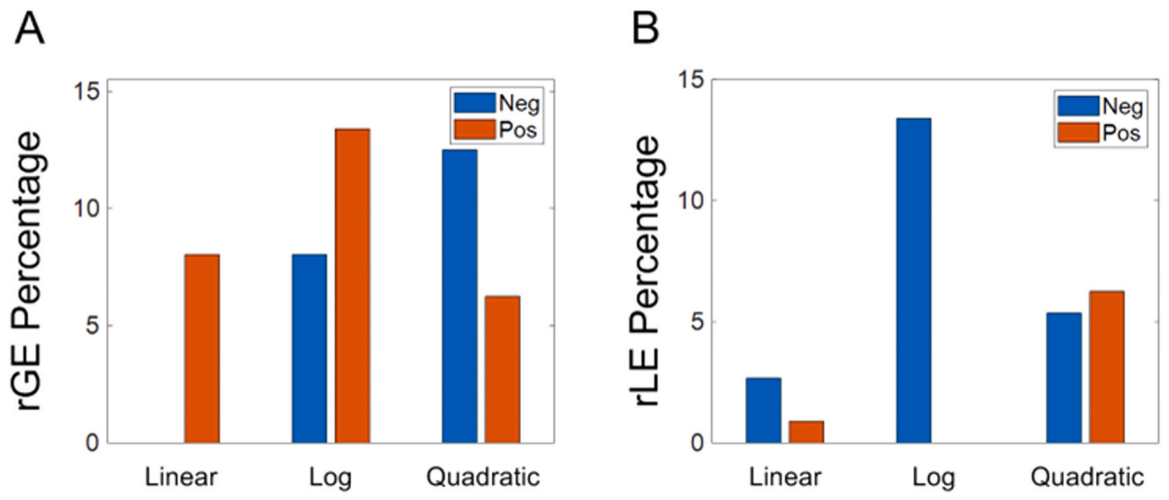

Fig. 4. The percentages of brain regions with significant age effects for each model of regional global efficiency (A) and regional local efficiency (B). Positive or negative T-values indicate an increase or decrease in developmental rate with age for the linear and logarithmic models, and U-shape or inverted U-shapes for the quadratic model, respectively. Neg: negative; Pos: positive.

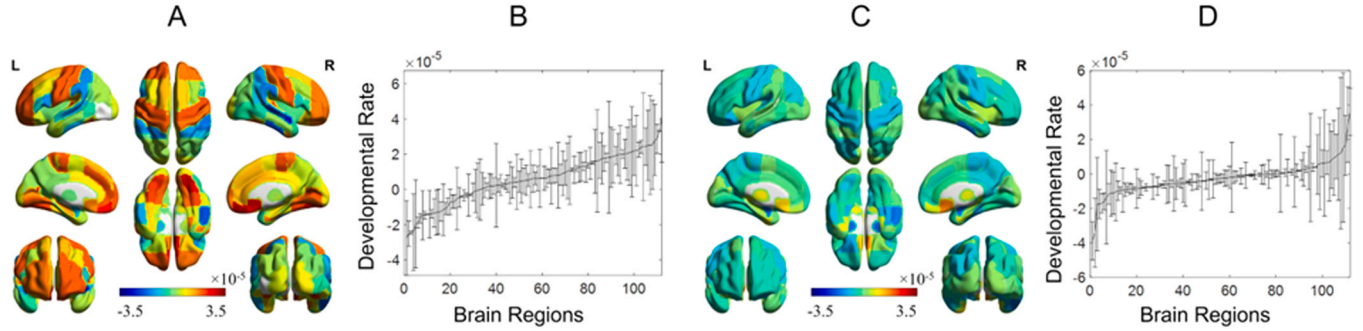

Fig. 5. The developmental rate maps of different regions (A and C) and their rankings (B and D) using a linear model for regional global efficiency (A and B) and regional local efficiency (C and D). Positive and negative values indicate increasing and decreasing developmental rates with age. The color bars in A and C represent the developmental rates, while the error bars in B and D denote the individual deviations.

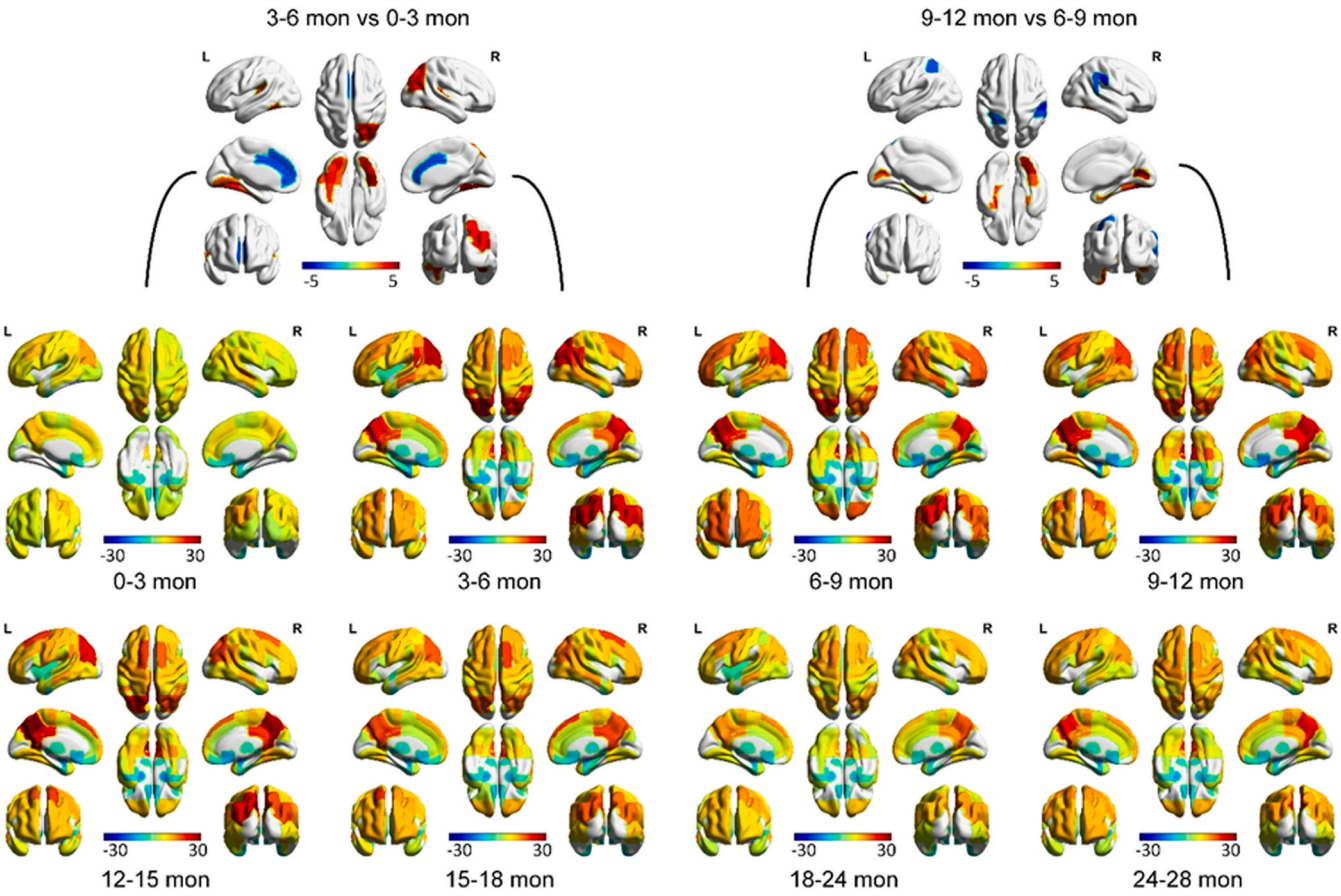

Fig. 6. The developmental comparison of regional global efficiency. The second and third rows display the brain regions significantly different from the individual whole-brain averages in each age group ($P < 0.05$, FDR corrected). The color bar presents the *T*-value of the paired t-test. Positive/negative *T*-values indicate above/below the individual whole-brain averages. The first row illustrates the significant brain regions in comparing two adjacent age groups ($P < 0.05$, FDR corrected). Positive/negative *T*-values indicate the extent to which the older age group is above/below the adjacent younger age group.

fusiform (TOF) showed a significant positive association with the ELC scores ($P < 0.05$, FDR corrected) and this association became weaker with age ($P < 0.05$, FDR corrected). The bilateral occipital fusiform gyri (OFG) were significantly and positively associated with ELC as well as ELS ($P < 0.05$, FDR corrected). Additionally, the right OFG showed a significant positive association with visual reception scores (VRS) while the left OFG was associated with receptive language scores (RLS) ($P < 0.05$, FDR corrected). Interestingly, all these associations were weakened with age ($P < 0.05$, FDR corrected). In contrast, only the log cognitive model revealed a negative association between the gross motor scores and the central opercular cortex (COC) ($P < 0.05$, FDR corrected) (Table 4). Again, this negative association became weaker with age ($P < 0.05$, FDR corrected).

3.6. Result validation

The aforementioned analyses utilized the AUC-based approach. To assess the reproducibility of our main results at different sparsity levels, we repeated the developmental trajectory analyses at three network sparsity levels: 17%, 28%, and 39%, representing the smallest, middle, and largest sparsity within the range that exhibited a small-world characteristic. Our results revealed similar developmental trajectories as those obtained using the AUC-based approach (Fig. S5 – S8).

4. Discussion

In this study, we used graph theory-derived efficiency attributes to investigate the development of brain functional networks during the first 28 months of life. By analyzing regional developmental trajectories, we confirmed our first hypothesis that the developmental trajectories of brain efficiency are spatially heterogeneous, revealing both linear and nonlinear age-related trajectories among different brain regions. Additionally, by examining the relationships between these regional developmental trajectories and cognitive abilities, we reported that the rGE developmental trajectories of the left TOF and bilateral OFG were associated with cognitive abilities. These findings could be essential for future clinical studies. For instance, our findings can be used to examine the efficiency development of specific brain regions, such as the left TOF and bilateral OFG, facilitating a better understanding and identification of potential neurodevelopmental abnormalities in infants and toddlers.

4.1. Developmental trajectories of whole-brain-based efficiency

Our result showed that the global efficiency of the whole brain increased non-linearly with age, while the local efficiency followed an inverted U-shaped trajectory. Increased global efficiency has been implicated to be associated with improved functional integration (Le et al., 2020), while local efficiency measures the degree of network segregation (Latora and Marchiori, 2001; Wang et al., 2009). Our GE results differed from those reported by Gao et al. (2011) who found significantly higher global efficiency in 1-year-olds when compared to infants at birth, while no differences were observed between 1 and 2 years old. The sparse sampling scheme employed by Gao et al. (2011) may have contributed to the observed discrepancies between the two studies.

The observed inverted U-shaped trajectory of local efficiency may

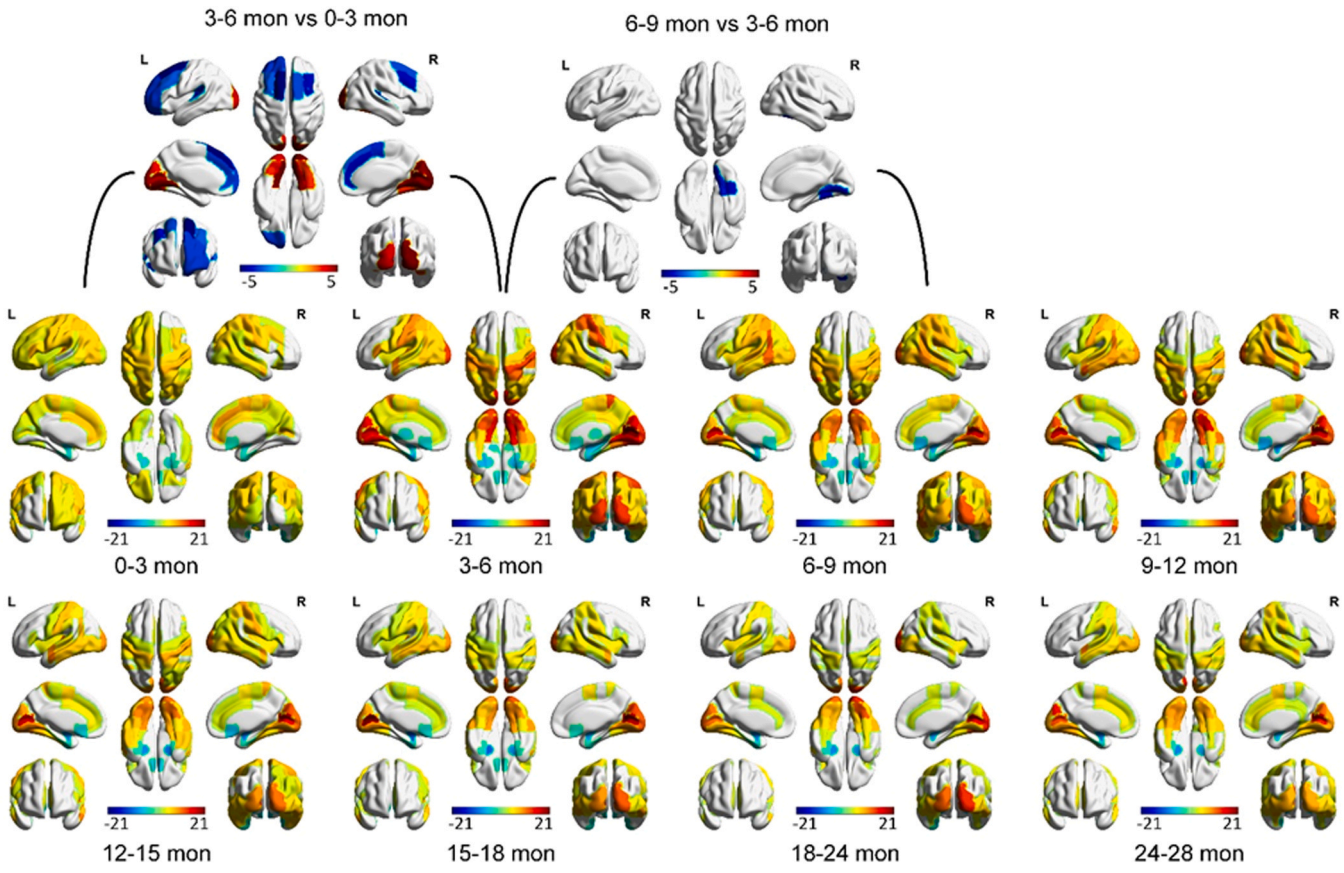

Fig. 7. The developmental comparison of regional local efficiency. The second and third rows show the brain regions significantly different from the individual whole-brain averages in each age group ($P < 0.05$, FDR corrected). The color bar presents the *T*-value of the paired t-test. Positive/negative *T*-values indicate above/below the individual whole-brain averages. The first row illustrates the significant brain regions comparing two adjacent age groups ($P < 0.05$, FDR corrected). Positive/negative *T*-values indicate the extent to which the older age group is above/below the adjacent younger age group.

Table 3
Significant association between cognitive scores and regional global efficiency development using a log cognitive model ($P < 0.05$, FDR corrected).

	OFG_L vs ELS				OFG_L vs RLS											
	β	*T*	*P*		*β*	*T*	*P*									
	TOF_L vs ELC				OFG_L vs ELC				OFG_L vs ELS				OFG_L vs RLS			
	β	*T*	*P*		*β*	*T*	*P*		*β*	*T*	*P*		*β*	*T*	*P*	
(Intercept)	0.0165	0.23	0.8173		0.0440	0.65	0.5130		0.0610	1.22	0.2224		0.1134	2.60	0.0096	
Site	0.0034	1.39	0.1647		0.0013	0.61	0.5400		0.0008	0.39	0.6962		0.0015	0.70	0.4841	
Gender	0.0042	1.90	0.0585		0.0000	-0.01	0.9957		-0.0001	-0	0.9754		0.0002	0.12	0.9018	
CogScore	9.46E-04	2.90	0.0039	*	0.0009	2.88	0.0041	*	0.0032	3.57	3.96E-04	*	0.0023	2.89	0.0040	*
ln(d)	0.0415	3.55	4.26E-04	*	0.0370	3.37	8.12E-04	*	0.0351	4.24	2.68E-05	*	0.0258	3.58	3.85E-04	*
ln(d):CogScore	-1.49E-04	-2.78	0.0057	*	-0.0001	-2.83	0.0049	*	-0.0005	-3.5	4.40E-04	*	-0.0004	-2.78	0.0057	*
	OFG_R vs ELC				OFG_R vs VRS				OFG_R vs ELS							
	β	*T*	*P*		*β*	*T*	*P*		*β*	*T*	*P*					
(Intercept)	0.0411	0.64	0.5198		0.0951	1.96	0.0502		0.0949	1.98	0.0487					
Site	-0.0004	-0.20	0.8416		-0.0005	-0.23	0.8155		-0.0010	-0.4	0.6653					
Gender	-0.0022	-1.16	0.2474		-0.0024	-1.23	0.2212		-0.0024	-1.2	0.2214					
CogScore	0.0008	2.83	0.0048	*	0.0022	2.63	0.0087	*	0.0023	2.66	0.0080	*				
ln(d)	0.0366	3.46	6.02E-04	*	0.0283	3.52	4.79E-04	*	0.0289	3.59	3.71E-04	*				
ln(d):CogScore	-0.0001	-2.72	0.0067	*	-0.0004	-2.56	0.0107	*	-0.0004	-2.6	0.0086	*				

*P < 0.05, FDR corrected. TOF: temporal occipital fusiform cortex; OFG: occipital fusiform gyrus; ELC: early learning compisite score; VRS: visual receptive score; RLS: receptive language score; ELS: expressive language score; L: left hemisphere; R: right hemisphere.

suggest that local functional segregation initially improves during early infancy, followed by a decrease in segregation with age during the first 28 months of life. Although many factors may explain this observed inverted U-shaped trajectory, one plausible explanation is the growth and elimination of superficial white matter U-fibers. Superficial white matter U-fibers are short connections that connect anatomical proximity regions, typically between neighboring gyri, surrounding the cortex sulci (Guevara et al., 2020; van Blooijs et al., 2023). These U-fibers can be clearly identified after the first three months of life (Hermoye et al., 2006). The development of superficial U-fibers from infancy to early childhood can be divided into three main stages (Hermoye et al., 2006): significant changes occur quickly within the first year, followed by

Table 4
Significant association between cognitive scores and regional local efficiency development using a log cognitive model (P < 0.05, FDR corrected).

	COC_R vs GMS			
	β	*T*	*P*	
(Intercept)	0.2198	22.85	3.46E-76	
Site	-3.47E-04	-0.40	0.6877	
Gender	0.0013	1.66	0.0969	
CogScore	-6.51E-04	-3.29	0.001103	*
ln(day)	-0.0071	-4.34	1.75E-05	*
ln(day):CogScore	1.09E-04	3.27	0.0011	*

* : P < 0.05 with FDR corrected. COC: central opercular cortex; GMS: gross motor score; R: right.

gradual alterations during the second year, and finally, relatively stable after 24 months old. This rapid proliferation of U-fibers in the early months of life could lead to increases of local connectivity which may enhance local efficiency. As U-fibers continue to develop and mature, they facilitate efficient communication and integration between nearby brain regions, resulting in a peak in local efficiency. However, as long-range connections begin to form and strengthen during early childhood (Cao et al., 2017; Gao et al., 2011), these long-range connections facilitate efficient communication between distant brain regions. As a result, the reliance on U-fibers for communication decreases, which in turn may lead to a decline in local efficiency. Therefore, the observed inverted U-shaped trajectory of local efficiency during the first 28 months of life could potentially reflect the dynamic interplay between the development and maturation of both short-range U-fibers and long-range connections in the brain.

Finally, we found that the whole-brain-based efficiency attributes did not show significant associations with cognitive ability, likely due to the observed spatiotemporally heterogeneous developmental trajectories of network efficiency during infancy.

4.2. Spatiotemporally heterogeneous development of regional efficiency

In addition to evaluating the whole brain efficiency developmental trajectories, one of the major focuses of our study was to characterize regional developmental trajectories of GE and LE. To this end, several of our key findings warrant additional discussion. First, the "sensorimotor stage" proposed by Piaget (Cherry, 2019; Piaget, 1973, 2013) characterizes rapid cognitive maturation from birth to approximately 2 years old, including both basic and more complex cognitive processes. During this stage, infants and toddlers coordinate sensory experiences (seeing, hearing) with motor actions (reaching, touching) to gain knowledge of their surroundings. Our results appear consistent with the maturation processes outlined in the "sensorimotor stage." Specifically, the primary sensorimotor regions showed a monotonic linear/log increase in rGE and a log decrease in rLE. More interestingly, bilateral frontal lobes showed a similar developmental pattern to that of the primary sensorimotor regions. The prefrontal cortex (PFC), which is a part of the neocortex, plays a crucial role in higher-order cognitive functions such as decision-making, planning, and working memory (Otero and Barker, 2013). As children near the conclusion of the sensorimotor stage and progress into the preoperational stage (2 – 7 years old, according to Piaget's theory), they demonstrate increasingly advanced cognitive capacities like engaging in symbolic play, engaging in pretend play, and utilizing mental representation (Cherry, 2019; Piaget, 1973, 2013). These abilities necessitate the engagement of brain regions within the frontal lobes (Kelly et al., 2011). Therefore, the observed increases of rGE and decreases of rLE in the sensorimotor areas and bilateral frontal lobes may reflect both basic and high-order cognitive development during the sensorimotor stage (Cherry, 2019; Piaget, 1973, 2013).

Second, the visual system rapidly matures at the onset of visual experience and continues throughout the first year of life, followed by a relatively stable trajectory after the first year of life (Hutter, 2021). The onset of visual experience is critical for shaping visual cortical circuits (Danka Mohammed and Khalil, 2020; Khalil et al., 2018). Gao et al. (2015b) found that the primary visual areas show a dramatic increase in BOLD signal synchronization during the first three months of life, followed by a slower increase. Our results confirm these findings in the primary visual areas (ScC and IcC) and adjacent higher-order visual areas (bilateral lingual and occipital fusiform gyrus), which showed a significant *log* increase of rGE. In addition, the rLE of the visual areas in the occipital lobe did not show significant age effects. Instead, these regions exhibited a stable rLE that is significantly higher than the whole brain average starting from the third month of life (Fig. 7), consistent with that observed by Yin et al. (2020), who reported that the voxels in the occipital visual areas remained closely connected with each other during infancy. Together, these findings suggested the presence of a segregated visual functional network with rapid increase of rGE during early infancy, followed by a stably high rGE afterward and a temporally stable but significantly higher rLE than that of the whole brain average LE.

Nevertheless, the rGE in the temporal/occipital visual areas exhibited an inverted U-shaped quadratic age effect (Fig. 3). These regions form the "what" circuit for high-order visual processing and are responsible for identifying objects (Hart Jr, 2015). The development of the "what" system is complex and influenced by the refinement of topographic projections within nuclei, columns within the cortex, and layers within the lateral geniculate nucleus (Daw, 2014). The inverted U-shaped trajectory of rGE may be initially attributed by the establishment of long-range connections across the "what" system (Yeatman et al., 2013), resulting in an enhanced functional integration. As the brain maturation continues, the "what" circuit may undergo specialization through the establishment of more local connections (Yin et al., 2020), leading to a decrease in global efficiency.

Finally, the posterior parietal extended to superior temporal associate areas showed decreasing log rGE development. Previous studies have indicated structural and functional intactness in the posterior parietal areas in 5–7-month-old infants (Wilcox et al., 2010). The strength of short-range connectivity increased faster than that of long-range connectivity in the parietal areas during infancy (Zhao et al., 2019b), which may account for the observed decreased rGE and increased rLE trend in our study. These findings may explain the observed pattern and serve as a foundation for the later long-range FC development.

4.3. Relationship between regional efficiency and cognitive abilities

The fusiform gyrus plays an important role in various visual-related tasks such as face recognition, color processing, and visual word form processing (Forseth et al., 2018; Grill-Spector and Weiner, 2014; Weiner and Grill-Spector, 2012). Previous research has shown that 2-month-old infants have color vision, enabling discrimination between colored targets and their surrounding stimulus fields, while those at 3-month-old can make discriminations based on color wavelength (Brown and Lindsey, 2013). Face-selective processes emerge in infants at 4–6 months (De Heering and Rossion, 2015), while 6- and 10-month infants can use top-down contextual information to guide attention orienting, object recognition, and visual search (Tummeltshammer and Amso, 2018). Moreover, the visual word form area in the fusiform gyrus is believed to be involved in identifying words and letters from lower-level shape images (Ostrolenk et al., 2017). A recent study reported a distinct neuroanatomical substrate in the middle fusiform gyrus that provides access to object semantic information (Forseth et al., 2018). Visual functions are critical to later behavioral and cognitive development, such as fine motor skill, attention, and language (D'souza et al., 2020; Maurer et al., 2007; Tsai et al., 2016). In this study, a positive association was found between the development of rGE in the left TOF and bilateral OFG, located in the fusiform gyrus, and early cognitive abilities. This finding suggests that strengthening information integration in

the fusiform visual regions may facilitate the development of higher-order cognitive abilities during the first years of life. Nevertheless, it should be noted that the observed associations between rGE and cognition were weakened with age increases.

For rLE, our study revealed a negative association between the central opercular cortex (COC) and gross motor scores using the nonlinear model. The COC is located near the precentral gyrus and has been linked to movement in individual participants (Eichert et al., 2021). These results suggest that young children with stronger gross motor abilities may have slower decreases in short-range functional connectivity with the COC, or that a slower decrease in short-range connectivity may lead to better gross motor abilities. However, this observed association weakened with age.

4.4. Limitations

Our study had several limitations that should be noted. First, although our results revealed spatially heterogeneous development of regional efficiency attributes, the biological mechanisms underlying this pattern remain largely unexplored. Second, this study focused solely on functional development without considering the morphological changes during early childhood. Future studies should consider both to fully understand the potential interplay between structural and functional development. Third, the age range was limited to 0–28 months in this study and future research will be needed to investigate the developmental patterns of efficiency attributes beyond this age range. Lastly, while our study employed Mullen cognitive ability measures, information on the developmental milestones of individual subjects, such as walking, speaking, reading, writing, and other high-order abilities, were not available, making it difficult to directly determine how the observed temporal and spatial characteristics of GE and LE could be related to these developmental milestones. Future studies focusing on the relations between rGE/rLE and developmental milestones could further improve our understanding of how graph theory-derived efficiency attributes can be used to gain insights into early-childhood brain development.

5. Conclusions

In this study, we analyzed high-quality brain functional connectome from a large-scale database to chart early brain functional development. Using graph theory, we identified key regions responsible for functional integration and coordination, as well as revealed patterns of spatially heterogeneous development in the infants' and toddlers' brains. Most intriguing, the regional global efficiency in the left temporal occipital fusiform and bilateral occipital fusiform gyrus but not whole brain global efficiency was found to be associated with early cognitive abilities, suggesting that regional efficiency is more sensitive in detecting brain – behavior associations than whole brain global parameters. This study provides new insights into the development of regional efficiency and its relationship with cognitive ability during early infancy.

Data and Code Availability Statement

The data included in this study are publicly available at the present time (https://nda.nih.gov/). We will be able to share all our codes on request.

Declaration of generative AI and AI-assisted technologies in the writing process

During the preparation of this work, the authors used ChatGPT to polish the writing of this manuscript. After using ChatGPT, the authors reviewed and edited the content as needed and take full responsibility for the content of the publication.

Declaration of Competing Interest

The authors declare that they have no known competing financial interests or personal relationships that could have appeared to influence the work reported in this paper.

Data availability

The data included in this study are publicly available online (https://nda.nih.gov/). We will be able to share all our codes on request.

Acknowledgment

This study was supported in part by NIH grants U01MH110274, MH104324–03S1 (JE), MH015755 (BH) and the efforts of the UNC/UMN Baby Connectome Project (BCP) Consortium.

Appendix A. Supporting information

Supplementary data associated with this article can be found in the online version at doi:10.1016/j.dcn.2023.101284.

References

Bagonis, M., Cornea, E., Girault, J.B., Stephens, R.L., Kim, S., et al., 2022. Early childhood development of node centrality in the white matter connectome and its relationship to iq at 6 years. BP: CNNI. https://doi.org/10.1016/j.bpsc.2022.09.005.
Bassett, D.S., Bullmore, E.T., 2017. Small-world brain networks revisited. Neuroscientist 23, 499–516. https://doi.org/10.1177/1073858416667720.
van Blooijs, D., van den Boom, M.A., van der Aar, J.F., Huiskamp, G.M., Castegnaro, G., et al., 2023. Developmental trajectory of transmission speed in the human brain. Nat. Neurosci. 1–5. https://doi.org/10.1038/s41593-023-01272-0.
Brown, A.M., Lindsey, D.T., 2013. Infant color vision and color preferences: A tribute to Davida Teller. Vis. Neurosci. 30, 243–250. https://doi.org/10.1017/S0952523813000114.
Bruchhage, M.M.K., Ngo, G.C., Schneider, N., D'Sa, V., Deoni, S.C.L., 2020. Functional connectivity correlates of infant and early childhood cognitive development. Brain Struct. Funct. 225, 669–681. https://doi.org/10.1007/s00429-020-02027-4.
Cafiero, R., Brauer, J., Anwander, A., Friederici, A.D., 2019. The concurrence of cortical surface area expansion and white matter myelination in human brain development. Cereb. Cortex 29, 827–837. https://doi.org/10.1093/cercor/bhy277.
Cao, H., McEwen, S.C., Forsyth, J.K., Gee, D.G., Bearden, C.E., et al., 2019. Toward leveraging human connectomic data in large consortia: generalizability of fMRI-Based brain graphs across sites, sessions, and paradigms. Cereb. Cortex 29, 1263–1279. https://doi.org/10.1093/cercor/bhy032.
Cao, M., Huang, H., He, Y., 2017. Developmental connectomics from infancy through early childhood. Trends Neurosci. 40, 494–506. https://doi.org/10.1016/j.tins.2017.06.003.
Cherry, K., 2019, The sensorimotor stage of cognitive development. Retrieved from verywellmind: ⟨https://www⟩. verywellmind. com/sensorimotor-stage-of-cognitive-development-2795462.
Danka Mohammed, C.P., Khalil, R., 2020. Postnatal development of visual cortical function in the mammalian brain. Front Syst. Neuroscie 14, 29. https://doi.org/10.3389/fnsys.2020.00029.
Daw, N.W., 2014. Anatomical Development of the Visual System. Visual Development. Springer US,, Boston, MA, pp. 55–76. https://doi.org/10.1007/978-1-4757-6940-1_4.
De Asis-Cruz, J., Bouyssi-Kobar, M., Evangelou, I., Vezina, G., Limperopoulos, C., 2015. Functional properties of resting state networks in healthy full-term newborns. Sci. Rep. 5, 17755. https://doi.org/10.1038/srep17755.
De Heering, A., Rossion, B., 2015. Rapid categorization of natural face images in the infant right hemisphere. Elife 4, e06564. https://doi.org/10.7554/eLife.06564.
Desikan, R.S., Segonne, F., Fischl, B., Quinn, B.T., Dickerson, B.C., et al., 2006. An automated labeling system for subdividing the human cerebral cortex on MRI scans into gyral based regions of interest. Neuroimage 31, 968–980. https://doi.org/10.1016/j.neuroimage.2006.01.021.
D'souza, D., D'Souza, H., Jones, E.J., Karmiloff-Smith, A., 2020. Attentional abilities constrain language development: A cross-syndrome infant/toddler study. Dev. Sci., e12961 https://doi.org/10.1111/desc.12961.
Eichert, N., Watkins, K.E., Mars, R.B., Petrides, M., 2021. Morphological and functional variability in central and subcentral motor cortex of the human brain. Brain Struct. Funct. 226, 263–279. https://doi.org/10.1007/s00429-020-02180-w.
Emerson, R.W., Gao, W., Lin, W., 2016. Longitudinal study of the emerging functional connectivity asymmetry of primary language regions during infancy. J. Neurosci. 36, 10883–10892. https://doi.org/10.1523/JNEUROSCI.3980-15.2016.
Eyre, M., Fitzgibbon, S.P., Ciarrusta, J., Cordero-Grande, L., Price, A.N., et al., 2021. The developing human connectome project: typical and disrupted perinatal functional connectivity. Brain 144, 2199–2213. https://doi.org/10.1093/brain/awab118.

Fan, Y., Shi, F., Smith, J.K., Lin, W., Gilmore, J.H., Shen, D., 2011. Brain anatomical networks in early human brain development. Neuroimage 54, 1862–1871.
Forseth, K.J., Kadipasaoglu, C.M., Conner, C.R., Hickok, G., Knight, R.T., et al., 2018. A lexical semantic hub for heteromodal naming in middle fusiform gyrus. Brain 141, 2112–2126. https://doi.org/10.1016/j.neuroimage.2010.07.025.
Fransson, P., Aden, U., Blennow, M., Lagercrantz, H., 2011. The functional architecture of the infant brain as revealed by resting-state fMRI. Cereb. Cortex 21, 145–154. https://doi.org/10.1093/cercor/bhq071.
Gao, W., Zhu, H.T., Giovanello, K.S., Smith, J.K., Shen, D.G., et al., 2009. Evidence on the emergence of the brain's default network from 2-week-old to 2-year-old healthy pediatric subjects. Proc. Natl. Acad. Sci. USA 106, 6790–6795. https://doi.org/10.1073/pnas.0811221106.
Gao, W., Gilmore, J.H., Giovanello, K.S., Smith, J.K., Shen, D., et al., 2011. Temporal and spatial evolution of brain network topology during the first two years of life. PLoS One 6, e25278. https://doi.org/10.1371/journal.pone.0025278.
Gao, W., Alcauter, S., Elton, A., Hernandez-Castillo, C.R., Smith, J.K., et al., 2015. Functional network development during the first year: relative sequence and socioeconomic correlations. Cereb. Cortex 25, 2919–2928. https://doi.org/10.1093/cercor/bhu088.
Gao, W., Lin, W., Grewen, K., Gilmore, J.H., 2017. Functional connectivity of the infant human brain: plastic and modifiable. Neuroscientist 23, 169–184. https://doi.org/10.1177/1073858416635986.
Gilmore, J.H., Knickmeyer, R.C., Gao, W., 2018. Imaging structural and functional brain development in early childhood. Nat. Revs Neurosci. 19, 123–137. https://doi.org/10.1038/nrn.2018.1.
Grill-Spector, K., Weiner, K.S., 2014. The functional architecture of the ventral temporal cortex and its role in categorization. Nat. Rev. Neurosci. 15, 536–548. https://doi.org/10.1038/nrn3747.
Guevara, M., Guevara, P., Román, C., Mangin, J.-F., 2020. Superficial white matter: A review on the dMRI analysis methods and applications. NeuroImage 212, 116673. https://doi.org/10.1016/j.neuroimage.2020.116673.
Hart Jr, J., 2015. The Neurobiology of Cognition and Behavior. Oxford University Press,.
Hedeker, D., Gibbons, R.D., 2006. Longitudinal Data Analysis. John Wiley & Sons,.
Hermoye, L., Saint-Martin, C., Cosnard, G., Lee, S.-K., Kim, J., et al., 2006. Pediatric diffusion tensor imaging: normal database and observation of the white matter maturation in early childhood. Neuroimage 29, 493–504. https://doi.org/10.1016/j.neuroimage.2005.08.017.
Howell, B.R., Styner, M.A., Gao, W., Yap, P.-T., Wang, L., et al., 2019. The UNC/UMN baby connectome project (BCP): an overview of the study design and protocol development. Neuroimage 185, 891–905. https://doi.org/10.1016/j.neuroimage.2018.03.049.
Huang, H., Shu, N., Mishra, V., Jeon, T., Chalak, L., et al., 2015. Development of human brain structural networks through infancy and childhood. Cereb. Cortex 25, 1389–1404. https://doi.org/10.1093/cercor/bht335.
Huang, Y., Wu, Z., Wang, F., Hu, D., Li, T., et al., 2022. Mapping developmental regionalization and patterns of cortical surface area from 29 post-menstrual weeks to 2 years of age. PNAS 119, e2121748119. https://doi.org/10.1073/pnas.2121748119.
Humphries, M.D., Gurney, K., 2008. Network 'small-world-ness': a quantitative method for determining canonical network equivalence. Plos One 3, e0002051. https://doi.org/10.1371/journal.pone.0002051.
Hutter, M., 2021, Learning curve theory. arXiv preprint arXiv:2102.04074. DOI: 10.48550/arXiv.2102.04074.
Jiang, W., Zhang, H., Hsu, L.-M., Hu, D., Li, G., et al., 2019. Early Development of Infant Brain Complex Network. International Conference on Medical Image Computing and Computer-Assisted Intervention. Springer,, pp. 832–840. https://doi.org/10.1007/978-3-030-32245-8_92.
Jiang, W., Merhar, S.L., Zeng, Z., Zhu, Z., Yin, W., et al., 2022. Neural alterations in opioid-exposed infants revealed by edge-centric brain functional networks. Brain Commun. 4, fcac112 https://doi.org/10.1093/braincomms/fcac112.
Kam, T.-E., Wen, X., Jin, B., Jiao, Z., Hsu, L.-M., et al., 2019. A deep learning framework for noise component detection from resting-state functional MRI. International Conference on Medical Image Computing and Computer-Assisted Intervention. Springer,, pp. 754–762. https://doi.org/10.1007/978-3-030-32248-9_84.
Kelly, R., Dissanayake, C., Ihsen, E., Hammond, S., 2011. The relationship between symbolic play and executive function in young children. AJEC 36, 21–27. https://doi.org/10.1177/18369391110360020.
Khalil, R., Contreras-Ramirez, V., Levitt, J.B., 2018. Postnatal refinement of interareal feedforward projections in ferret visual cortex. Brain Struct. Funct. 223, 2303–2322. https://doi.org/10.1007/s00429-018-1632-2.
King, T., 2016. Longitudinal data analysis for the behavioral sciences using R. Int. J. Lang. Commun. Disord. 51, 355-355. https://doi.org/10.1111/1460-6984.12194.
Latora, V., Marchiori, M., 2001. Efficient behavior of small-world networks. Phys. Rev. Lett. 87. https://doi.org/10.1103/PhysRevLett.87.198701.
Le, T.M., Huang, A.S., O'Rawe, J., Leung, H.-C., 2020. Functional neural network configuration in late childhood varies by age and cognitive state. Dev. Cogn. Neurosci. 45, 100862 https://doi.org/10.1016/j.dcn.2020.100862.
Maurer, D., Mondloch, C.J., Lewis, T.L., 2007. Effects of early visual deprivation on perceptual and cognitive development. Prog. Brain Res 164, 87–104. https://doi.org/10.1016/S0079-6123(07)64005-9.
Mullen, E.M., 1995. Mullen Scales of Early Learning. AGS Circle Pines, MN,.
Nie, J., Li, G., Wang, L., Shi, F., Lin, W., et al., 2014. Longitudinal development of cortical thickness, folding, and fiber density networks in the first 2 years of life. Hum. Brain Mapp. 35, 3726–3737. https://doi.org/10.1002/hbm.22432.
Ostrolenk, A., Forgeot d'Arc, B., Jelenic, P., Samson, F., Mottron, L., 2017. Hyperlexia: Systematic review, neurocognitive modelling, and outcome. Neurosci. Biobehav Rev. 79, 134–149. https://doi.org/10.1016/j.neubiorev.2017.04.029.
Otero, T.M., Barker, L.A., 2013. The frontal lobes and executive functioning. Handbook of Executive Functioning. Springer,, pp. 29–44.
Peterson, M.R., Cherukuri, V., Paulson, J.N., Ssentongo, P., Kulkarni, A.V., et al., 2021. Normal childhood brain growth and a universal sex and anthropomorphic relationship to cerebrospinal fluid. J. Neurosurg. Pedia 28, 458–468. https://doi.org/10.3171/2021.2.PEDS201006.
Piaget, J., 1973. The Child's Conception of the World: Transl. by Joan and Andrew Tomlinson. Paladin,.
Piaget, J., 2013. Child's Conception of Movement and Speed. Routledge,.
Power, J.D., Barnes, K.A., Snyder, A.Z., Schlaggar, B.L., Petersen, S.E., 2012. Spurious but systematic correlations in functional connectivity MRI networks arise from subject motion. Neuroimage 59, 2142–2154. https://doi.org/10.1016/j.neuroimage.2011.10.018.
Ratnarajah, N., Rifkin-Graboi, A., Fortier, M.V., Chong, Y.S., Kwek, K., et al., 2013. Structural connectivity asymmetry in the neonatal brain. Neuroimage 75, 187–194. https://doi.org/10.1016/j.neuroimage.2013.02.052.
Tang, Y., Jiang, W., Liao, J., Wang, W., Luo, A., 2013. Identifying individuals with antisocial personality disorder using resting-state FMRI. Plos One 8, e60652. https://doi.org/10.1371/journal.pone.0060652.
Tsai, L.T., Hsu, J.L., Wu, C.T., Chen, C.C., Su, Y.C., 2016. A new visual stimulation program for improving visual acuity in children with visual impairment: a pilot study. Front Hum. Neurosci. 10, 157. https://doi.org/10.3389/fnhum.2016.00157.
Tummeltshammer, K., Amso, D., 2018. Top-down contextual knowledge guides visual attention in infancy. Dev. Sci. 21, e12599 https://doi.org/10.1111/desc.12599.
Tymofiyeva, O., Hess, C.P., Ziv, E., Lee, P.N., Glass, H.C., et al., 2013. A DTI-based template-free cortical connectome study of brain maturation. Plos One 8, e63310. https://doi.org/10.1371/journal.pone.0063310.
Wang, F., Lian, C., Wu, Z., Zhang, H., Li, T., et al., 2019. Developmental topography of cortical thickness during infancy. PNAS 116, 15855–15860. https://doi.org/10.1073/pnas.1821523116.
Wang, J., Wang, L., Zang, Y., Yang, H., Tang, H., et al., 2009. Parcellation-dependent small-world brain functional networks: A resting-state fMRI study. Hum. Brain Mapp. 30, 1511–1523. https://doi.org/10.1002/hbm.20623.
Wang, J., Qiu, S., Xu, Y., Liu, Z., Wen, X., et al., 2014. Graph theoretical analysis reveals disrupted topological properties of whole brain functional networks in temporal lobe epilepsy. Clin. Neurophysiol. 125, 1744–1756. https://doi.org/10.1016/j.clinph.2013.12.120.
Wang, L., Gao, Y., Shi, F., Li, G., Gilmore, J.H., et al., 2015. LINKS: learning-based multi-source IntegratioN frameworK for Segmentation of infant brain images. Neuroimage 108, 160–172. https://doi.org/10.1016/j.neuroimage.2014.12.042.
Wang, L., Wu, Z., Chen, L., Sun, Y., Lin, W., et al., 2023. iBEAT V2.0: a multi-site applicable, deep learning-based pipeline for infant cerebral cortical surface reconstruction. Nat. Protoc. https://doi.org/10.1038/s41596-023-00806-x.
Watts, D.J., Strogatz, S.H., 1998. Collective dynamics of 'small-world' networks. Nature 393, 440–442. https://doi.org/10.1038/30918.
Weiner, K.S., Grill-Spector, K., 2012. The improbable simplicity of the fusiform face area. Trends Cogn. Sci. 16, 251–254. https://doi.org/10.1016/j.tics.2012.03.003.
Wen, X., Zhang, H., Li, G., Liu, M., Yin, W., et al., 2019. First-year development of modules and hubs in infant brain functional networks. Neuroimage 185, 222–235. https://doi.org/10.1016/j.neuroimage.2018.10.019.
Wen, X., Wang, R., Yin, W., Lin, W., Zhang, H., et al., 2020. Development of dynamic functional architecture during early infancy. Cereb. Cortex 30 (11), 5626–5638. https://doi.org/10.1093/cercor/bhaa128.
Wilcox, T., Haslup, J.A., Boas, D.A., 2010. Dissociation of processing of featural and spatiotemporal information in the infant cortex. NeuroImage 53, 1256–1263. https://doi.org/10.1016/j.neuroimage.2010.06.064.
Wu, G., Wang, Q., Shen, D., 2012. Registration of longitudinal brain image sequences with implicit template and spatial-temporal heuristics. Neuroimage 59, 404–421. https://doi.org/10.1016/j.neuroimage.2011.07.026.
Yan, C., He, Y., 2011. Driving and driven architectures of directed small-world human brain functional networks. PLoS One 6, e23460. https://doi.org/10.1371/journal.pone.0023460.
Yap, P.T., Fan, Y., Chen, Y., Gilmore, J.H., Lin, W., et al., 2011. Development trends of white matter connectivity in the first years of life. PLoS One 6, e24678. https://doi.org/10.1371/journal.pone.0024678.
Yeatman, J.D., Rauschecker, A.M., Wandell, B.A., 2013. Anatomy of the visual word form area: adjacent cortical circuits and long-range white matter connections. Brain Lang. 125, 146–155. https://doi.org/10.1016/j.bandl.2012.04.010.
Yin, W., Chen, M.-H., Hung, S.-C., Baluyot, K.R., Li, T., et al., 2019. Brain functional development separates into three distinct time periods in the first two years of life. Neuroimage 189, 715–726. https://doi.org/10.1016/j.neuroimage.2019.01.025.
Yin, W., Li, T., Hung, S.C., Zhang, H., Wang, L., et al., 2020. The emergence of a functionally flexible brain during early infancy. Proc. Natl. Acad. Sci. USA 117, 23904–23913. https://doi.org/10.1073/pnas.2002645117.
Yitzhak, N., Harel, A., Yaari, M., Friedlander, E., Yirmiya, N., 2016. The Mullen scales of early learning: ceiling effects among preschool children. Eur. J. Dev. Psychol. 13, 138–151. https://doi.org/10.1080/17405629.2015.1073584.
Zhang, H., Shen, D.G., Lin, W.L., 2019. Resting-state functional MRI studies on infant brains: A decade of gap-filling efforts. Neuroimage 185, 664–684. https://doi.org/10.1016/j.neuroimage.2018.07.004.
Zhao, T., Xu, Y., He, Y., 2019a. Graph theoretical modeling of baby brain networks. NeuroImage 185, 711–727. https://doi.org/10.1016/j.neuroimage.2018.06.038.

Zhao, T., Mishra, V., Jeon, T., Ouyang, M., Peng, Q., et al., 2019b. Structural network maturation of the preterm human brain. NeuroImage 185, 699–710. https://doi.org/10.1016/j.neuroimage.2018.06.047.

Zhou, Z., Chen, X., Zhang, Y., Hu, D., Qiao, L., et al., 2020. A toolbox for brain network construction and classification (BrainNetClass. Hum. brain Mapp. 41, 2808–2826. https://doi.org/10.1002/hbm.24979.

Ziegler, G., Dahnke, R., Jäncke, L., Yotter, R.A., May, A., et al., 2012. Brain structural trajectories over the adult lifespan. Hum. Brain Mapp. 33, 2377–2389. https://doi.org/10.1002/hbm.21374.